

# Manifestations of the Efimov Effect for Three Identical Bosons

J. P. D’Incao and B. D. Esry

*Department of Physics, Kansas State University, Manhattan, Kansas 66506*

In this paper we present results from numerical calculations for three identical boson systems for both very large and infinite two-body  $s$ -wave scattering length  $a$ . We have considered scattering lengths up to  $2 \times 10^5$  a.u. and solved the hyperangular part of the Schrödinger equation for distances up to  $10^6$  a.u.. From these, we obtained the three-body effective potentials, hyperspherical channel functions and the asymptotic behavior of the nonadiabatic couplings in order to characterize the main aspects of the Efimov states. These results allow us to test and quantify the assumptions related to the Efimov effect.

PACS numbers: 34.50.-s,31.15.Ja,34.20.Gj

## I. INTRODUCTION

The experimental ability to create ultracold atomic systems, such as Bose-Einstein condensates, with a large range of interaction strengths has raised the possibility of investigating a very unusual phenomenon: the Efimov effect. The Efimov effect [1] is responsible for the emergence of an attractive long-range effective three-body interaction irrespective of the short-range character of the atomic interactions, producing a large number of three-body bound states — called Efimov states — even when the two-body subsystems have none. This effect is expected to occur in the limit where the two-body  $s$ -wave scattering length  $a$  is much larger than the characteristic range  $r_0$  of the interatomic interactions. Such a regime can be reached, for instance, by tuning the two-body interactions via an external magnetic field near a Feshbach resonance [2, 3, 4, 5, 6]. Besides its intriguing impact on the three-body bound state spectrum, Efimov physics has been invoked to explain the remarkable universality of three-body scattering observables at ultracold energies [7, 8, 9, 10, 11, 12, 13, 14]. Here, we use the less restrictive term “Efimov physics” to indicate the qualitative change in behavior exhibited by the system when  $|a| \rightarrow \infty$ .

Despite their importance, neither Efimov states nor any other signature of Efimov physics has yet been detected. The main difficulty for direct observation of these states stems from the fact that the Efimov states are very weakly bound and easily perturbed. Indirect observation of Efimov physics might be possible, however, by measuring some three-body scattering observables like three-body recombination or vibrational relaxation [7, 8, 9, 10, 11, 12] as a function of the scattering length. The detection of the series of interference minima and resonance peaks present in the three-body recombination rate as a function  $a$ , or of the resonance peaks in the vibrational relaxation rate, would be a clear signature of the Efimov physics involved in the ultracold three-body collisions. In this case, the main difficulties arise from the fact that finite collision energies — even ultracold energies — reduce the range of  $a$  in which Efimov physics can be observed [12]. At finite

energies, the unitary limit, high partial waves, and thermal averaging tend to wash out the features connected to Efimov physics. The coldest current experiments, however, might offer a large enough window in scattering length to see Efimov physics, but they would still be difficult experiments. For Bose-Einstein condensates of  $^4\text{He}$ ,  $^{23}\text{Na}$  and  $^{87}\text{Rb}$ , for instance, we can expect to observe at most three interference minima or resonance peaks in the three-body recombination rate for energies of 3 nK, 0.5 nK and 0.1 nK, respectively [12]. To see more than three of either requires even lower temperatures.

Previous theoretical work [7, 8, 9, 10, 11, 12] has revealed many universal low-energy three-body scattering properties related to Efimov physics. In this regime, the effective interactions and the three-body observables are determined primarily by  $a$ , independent of the details of the two-body interactions. The assumption that the attractive long-range behavior of the three-body effective potential ( $\propto -1/R^2$ ) is valid in the range  $r_0 \ll R \ll |a|$ , with  $R$  giving the overall size of the three-body system, is usually required in order to determine the  $a$  dependence in the three-body observables. In fact, the more relaxed assumption that this potential holds even for  $r_0 \lesssim R \lesssim |a|$  has been used to deduce the number of Efimov states and other low-energy three-body observables [9, 10, 11, 14]. Neither assumption, however, has been thoroughly tested against accurate calculations. Given the central role these assumptions play in determining the universal properties of ultracold three-body scattering, they should be tested.

For this paper, we have solved the Schrödinger equation for three identical bosons using the adiabatic hyperspherical representation for the  $J^\pi = 0^+$  symmetry over a broad range of scattering lengths, including essentially infinite values. The numerical results were obtained in a regime not accessible in previous calculations, allowing us to test the assumptions above by checking the modifications to the effective three-body potentials as  $|a| \rightarrow \infty$ . In addition, we have explored the validity of the above assumptions as the number of two-body bound states in the two-body potential is increased. We have considered both positive and negative scattering lengths, up to  $2 \times 10^5$  a.u. in magnitude and separately the infinite  $a$  case. We solved the three-body Schrödinger equation for

distances  $R$  as large as  $10^6$  a.u. in order to determine the effective three-body potentials as well as the nonadiabatic couplings responsible for inelastic transitions. The asymptotic behavior of the coupling and the hyperspherical channel functions was investigated to point out the main characteristics of the Efimov states in the adiabatic hyperspherical point of view.

## II. ADIABATIC HYPERSPHERICAL REPRESENTATION

We solve the three-body Schrödinger equation using the adiabatic hyperspherical representation [15, 16]. After the usual separation of the center-of-mass motion, the three-body problem can be described by the hyperradius  $R$  and five angles, denoted collectively by  $\Omega$ . The five angular coordinates are chosen to be the Euler angles ( $\alpha$ ,  $\beta$  and  $\gamma$ ) that specify the orientation of the the plane defined by the three particles relative to the space-fixed frame, plus two hyperangles ( $\varphi$  and  $\theta$ ) defined as a modification of Smith-Whitten coordinates [15, 16, 17].

The Schrödinger equation in hyperspherical coordinates can be written in terms of the rescaled wave function  $\psi = R^{5/2}\Psi$  (in atomic units),

$$\left[ -\frac{1}{2\mu} \frac{\partial^2}{\partial R^2} + H_{\text{ad}}(R, \Omega) \right] \psi(R, \Omega) = E\psi(R, \Omega), \quad (1)$$

where  $\mu$  is the three-body reduced mass (we choose  $\mu =$

$m/\sqrt{3}$  for three identical bosons of mass  $m$ ) and  $E$  is the total three-body energy. The adiabatic Hamiltonian  $H_{\text{ad}}$  is given by

$$H_{\text{ad}}(R, \Omega) = \frac{\Lambda^2(\Omega) + \frac{15}{4}}{2\mu R^2} + V(R, \varphi, \theta), \quad (2)$$

in which  $\Lambda^2$  is the grand angular momentum operator and  $V$  contains the interparticle interactions.

In the adiabatic hyperspherical representation, the total wave function is expanded on the channel functions  $\Phi_\nu(R; \Omega)$ ,

$$\psi(R, \Omega) = \sum_\nu F_\nu(R) \Phi_\nu(R; \Omega), \quad (3)$$

where the expansion coefficient  $F_\nu(R)$  is the hyperradial wave function. The total wave function is still, in principle, exact. The channel functions  $\Phi_\nu(R; \Omega)$  form a complete set of orthonormal functions at each  $R$  and are eigenfunctions of the adiabatic Hamiltonian:

$$H_{\text{ad}}(R, \Omega) \Phi_\nu(R; \Omega) = U_\nu(R) \Phi_\nu(R; \Omega). \quad (4)$$

The eigenvalues of this equation,  $U_\nu(R)$ , play the role of effective potentials for the hyperradial motion. This fact can be seen upon substitution of Eq. (3) into the Schrödinger equation (1) and projecting out  $\Phi_\nu$ . The result is a system of coupled ordinary differential equations

$$\left[ -\frac{1}{2\mu} \frac{d^2}{dR^2} + U_\nu(R) \right] F_\nu(R) - \frac{1}{2\mu} \sum_{\nu'} \left[ 2P_{\nu\nu'}(R) \frac{d}{dR} + Q_{\nu\nu'}(R) \right] F_{\nu'}(R) = EF_\nu(R), \quad (5)$$

where  $P_{\nu\nu'}(R)$  and  $Q_{\nu\nu'}(R)$  are the nonadiabatic coupling terms. These couplings are generated by the  $R$ -dependence of the channel functions and are responsible for the inelastic transitions in three-body scattering. They are defined as

$$P_{\nu\nu'}(R) = \left\langle \left\langle \Phi_\nu(R) \left| \frac{d}{dR} \right| \Phi_{\nu'}(R) \right\rangle \right\rangle \quad (6)$$

and

$$Q_{\nu\nu'}(R) = \left\langle \left\langle \Phi_\nu(R) \left| \frac{d^2}{dR^2} \right| \Phi_{\nu'}(R) \right\rangle \right\rangle, \quad (7)$$

where the double brackets denote integration over the angular coordinates  $\Omega$  only. Here, we will concentrate the solutions of the adiabatic equation (4), namely the potential curves and couplings. For the present calculations, the potential  $V$  in Eq. (2) is a pairwise sum of short-range potentials,  $V = v(r_{12}) + v(r_{31}) + v(r_{23})$ , which is a good model for spin-stretched atoms.

### A. Two-body potential model

To a good approximation, the Efimov effect, as well as other low-energy three-body properties, do not depend on the details of the interatomic interaction, only on the scattering length and  $r_0$ , the characteristic range of the interatomic interactions. This approximation, verified for different two-body potentials [7], allows the use of model potentials, substantially simplifying the numerical calculations by controlling the number of two-body channels in the problem. The two-body potential adopted here is  $v(r) = D \text{sech}^2(r/r_0)$ . With this potential, we can easily produce two-body systems with different values of the scattering length by changing the interaction strength  $D$ . The scattering length is determined for each value of  $D$  by solving the two-body scattering problem. For infinite values of the scattering length, however, we used a slightly different approach which will be discussed in more detail below. We have considered potentials with

just one two-body bound state and a characteristic range of  $r_0 = 15$  a.u., and using the mass of  ${}^4\text{He}$  atoms.

Figure 1 shows the scattering length  $a$  as a function of the potential strength  $D$ . Each time that the two-body potential deepens enough to support an additional  $s$ -wave bound state, the scattering length goes through a pole, labeled in Fig. 1 by  $D_I$ ,  $D_{II}$  and  $D_{III}$ . For  $D > D_I$ , the two-body system has no bound state and represents the standard Efimov case when  $|a| \rightarrow \infty$ . For  $D_{II} < D < D_I$ , the system has a single  $s$ -wave bound state, and for  $D_{III} < D < D_{II}$ , the system has gained another  $s$ -wave bound state. Our model two-body potential mimics the magnetic field control of the scattering length near a two-body  $s$ -wave Feshbach resonance [2, 3, 4, 5, 6], assuming that the only effect the resonance is to change the scattering length. In fact, we expect this model to be valid in the threshold regime, i.e., when the collision energy is the smallest energy in the system [12]. As  $a \rightarrow +\infty$ , the two-body bound state is weakly bound, and the three-body effective potential that approaches this state asymptotically supports the three-body Efimov states. As  $a \rightarrow -\infty$ , the two-body bound state becomes a deep bound state and the Efimov states are resonances rather than bound states.

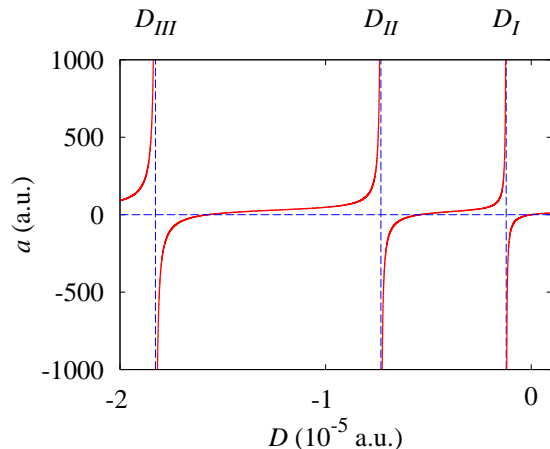


FIG. 1: The two-body  $s$ -wave scattering length  $a$  as a function of the potential strength  $D$ . When the two-body potential is deep enough to support an additional bound state,  $a$  passes through a pole, indicated by  $D_I$ ,  $D_{II}$  and  $D_{III}$ .

To determine the value of  $D$  that gives a particular scattering length, we simply read the value from Fig. 1. To determine the value of  $D$  that gives  $|a| \rightarrow \infty$  from the figure, though, is not simple to do accurately. We thus used a slightly different approach that takes advantage of the fact that the derivative of the two-body radial wave function must vanish at large distances when  $|a| = \infty$ . To this end, we solved the two-body radial Schrödinger equation at zero energy,

$$\left[ -\frac{1}{m} \frac{d^2}{dr^2} + D \text{sech}^2(r/r_0) \right] u(r) = 0, \quad (8)$$

and required  $u'(r) = 0$  at some large distance. The potential strength  $D$  is the eigenvalue of Eq. (8) — the low-

est corresponds to the solution with no nodes  $D = D_I$ , the next to the solution with one node  $D = D_{II}$ , and so on. This procedure determines  $D$  to essentially machine precision. We can then perform three-body calculations with a scattering length as close as numerically possible to infinity.

It is worth noting that the solutions of the  $\text{sech}^2$  potential are known analytically, so that we could, in principle, determine these values of  $D$  exactly. We used the present method because it will work for any short-range potential.

## B. Effective hyperspherical potentials

Neglecting all off-diagonal terms in Eq. (5) defines the effective hyperspherical potential,

$$W_\nu(R) = U_\nu(R) - \frac{1}{2\mu} Q_{\nu\nu}(R). \quad (9)$$

For short-range two-body potentials the channel index  $\nu$  labels both two-body and three-body configurations in the asymptotic limit ( $R \rightarrow \infty$ ). In this limit, the potential curves  $U_\nu(R)$  approach either a two-body bound state energy for the bound channels (BC) or zero energy for the three-body continuum channels (CC). In both cases,  $Q_{\nu\nu}$  vanishes for  $R \rightarrow \infty$ .

For finite  $a$ , however, the effective potentials are influenced by Efimov physics in the range  $r_0 \ll R \ll |a|$ . For these  $R$ , the effective potentials are proportional to  $R^{-2}$ , and can be attractive or repulsive. The channel of primary interest in this case is the one that leads to the Efimov effect — for  $a > 0$ , it is the channel correlated asymptotically with the weakly bound  $s$ -wave dimer; for  $a < 0$ , it is the lowest continuum channel. Because of its importance in our discussion we label it the “Efimov channel” (EC). It is worth to mention that for  $R \gg |a|$  the Efimov channel behaves as a bound or continuum channel, as appropriate.

In Fig. 2 we show the effective potentials  $W_\nu(R)$  calculated near the pole  $D = D_I$  in Fig. 1. For  $a > 0$ , the lowest potential is the Efimov channel (EC), converging to the two-body bound state for  $R \rightarrow \infty$ . The higher lying potentials are associated with three-body continuum channels (CC). As  $D$  is increased towards  $D_I$  from the left,  $a \rightarrow +\infty$  and the dimer binding energy vanishes. At the same time, the Efimov channel evolves from that shown in Fig. 2 to a purely attractive  $R^{-2}$  for  $R \gg r_0$ . Similarly, for  $a < 0$  in Fig. 2(b), the lowest potential is the Efimov channel (EC) converging to the three-body continuum limit as  $R \rightarrow \infty$ . In this case,  $a \rightarrow -\infty$  as  $D$  approaches  $D_I$  from the right, and the potential barrier in the Efimov channel moves to infinity ( $R \propto |a|$ ). At  $D = D_I$ , the potential is the same attractive  $R^{-2}$  obtained by approaching  $D_I$  from the left. Note that for both  $a < 0$  and  $a > 0$ , there can be bound channels (BC) that lie at lower energies.

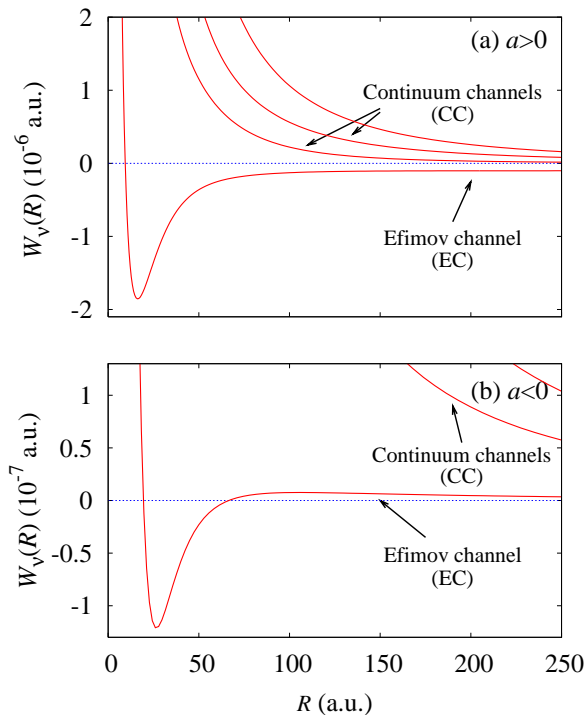


FIG. 2: The three-body effective potential for (a)  $a > 0$  and (b)  $a < 0$ , calculated near pole  $D = D_I$ . For  $a > 0$ , the system has only one bound state, while for  $a < 0$  the system has none.

The asymptotic behavior,  $R \gg |a|$ , of the effective potential  $W_\nu(R)$  can be determined analytically [18, 19]. For the bound channels (BC), the asymptotic limit represents the atom-dimer configuration, and the asymptotic effective potential is given by

$$W_\nu(R) = E_{v'l'} + \frac{l(l+1)}{2\mu R^2} + \mathcal{O}\left(\frac{1}{R^3}\right). \quad (10)$$

The rovibrational energy  $E_{v'l'}$  of the dimer is labeled by its vibrational quantum number  $v$  and its angular momentum  $l'$ ;  $l$  is the relative angular momentum between the dimer and the third atom. The notation  $\mathcal{O}(\dots)$  indicates the leading order correction.

The three-body continuum channels (CC) represent three free atoms, each one far from the others in the asymptotic limit. The two-body potentials thus vanish, leaving only the kinetic energy. Therefore, the leading term of the effective potential is determined by the eigenvalues  $\lambda(\lambda+4)$  of the kinetic energy, and the higher order terms can be written in terms of the scattering length  $a$ ,

$$W_\nu(R) = \frac{\lambda(\lambda+4) + \frac{15}{4}}{2\mu R^2} + \frac{c_1}{\mu R^2} \left(\frac{a}{R}\right)^{2l_0+1} + \frac{c_2}{\mu R^2} \left(\frac{a}{R}\right)^{2l_0+2} + \mathcal{O}\left(\frac{1}{R^{2l_0+5}}\right), \quad (11)$$

where  $c_1$  and  $c_2$  are positive constants. We can relate the quantum number  $\lambda$  to the partial angular momenta of the

system using  $\lambda = 2n + l + l' - n$  is a non-negative integer,  $l'$  is the angular momentum associated with the Jacobi vector connecting particles 1 and 2 and  $l$  with the Jacobi vector connecting particle 3 with the center of mass of 1 and 2 [see also Eq. (10)]. For identical bosons with  $J^\pi = 0^+$ , symmetry requires  $\lambda = 0, 4, 6, \dots$ , and  $l = l' = 0, 2, 4, \dots$ . The quantum number  $l_0$  in Eq. (11) can thus be thought of as the dominant partial wave in the expansion of a continuum state labeled by  $\lambda$ . It is non-zero only when there are degeneracies in  $\lambda$  — which begin in the present case with  $\lambda = 12$ . Thus, this situation does not occur for the lowest continuum channel which is usually of most interest for ultracold collisions. We will use  $\lambda$  and  $l_0$  to label the three-body continuum channels

As discussed above for  $|a| \rightarrow \infty$ , the effective potentials for both  $a < 0$  and  $a > 0$  in the range  $r_0 \ll R \ll |a|$  are proportional to  $R^{-2}$ . Explicitly,

$$W_\nu(R) = -\frac{s_\nu^2 + \frac{1}{4}}{2\mu R^2} + \mathcal{O}\left(\frac{1}{R^3}\right), \quad (12)$$

with  $s_\nu = 1.00624$ , therefore producing an infinite number of three-body bound states when  $|a| = \infty$  — which is precisely the Efimov effect. The higher-lying continuum channels also feel the influence of the Efimov physics and are no longer associated simply with the eigenvalues of the kinetic energy. For  $r_0 \ll R \ll |a|$ , they are given by

$$W_\nu(R) = \frac{s_\nu^2 - \frac{1}{4}}{2\mu R^2} + \mathcal{O}\left(\frac{1}{R^3}\right), \quad (13)$$

where  $s_\nu$  is a constant that represents a sort of correlation in addition to the kinetic energy.

In some way, the assumption that the potentials (12) and (13) hold for  $r_0 \ll R \ll |a|$ , has been used [9, 10, 11, 14] to deduce many properties of three-body systems with a large scattering length. In fact, it was the more relaxed assumption that the long-range effective potential (12) holds even for  $r_0 \lesssim R \lesssim |a|$  that was used in Refs. [9, 10, 11, 14] to deduce some low-energy three-body observables and the number of Efimov states,

$$N \simeq (s_0/\pi) \ln(|a|/r_0). \quad (14)$$

The validity of the assumption that  $r_0 \lesssim R \lesssim |a|$  sets limits on the quantitative aspects of these predictions. In the next section, the above assumptions will be tested with accurate numerical calculations for scattering lengths up to 200000 a.u. (and  $r_0 = 15$  a.u.), which is unambiguously in the regime  $|a| \gg r_0$ .

### III. RESULTS AND DISCUSSION

The adiabatic equation (4) has been solved for hyper-radii up to  $2 \times 10^6$  a.u. in order to reach the asymptotic regime for the effective potential and couplings. We can thus compare our numerical results with the common assumptions of the Efimov effect. The main thrust

of this investigation is to establish quantitative bounds on the range where the Efimov potential accurately approximates the effective potential. In addition, we have investigated the qualitative differences between Efimov states and ordinary three-body bound states by analyzing the channel function and nonadiabatic couplings when  $|a| \rightarrow \infty$ .

### A. Effective Potentials

We show in Fig. 3 the effective potentials associated with the weakly bound dimer for  $a > 0$ , and with lowest continuum channel for  $a < 0$ , for several values of  $a$ . They are multiplied by the factor  $2\mu R^2$  in order to more clearly reveal whether they match Eq. (12). If Eq. (12) holds, then these curves should approach the constant  $-s_0^2 (= 1.0125)$ . Figure 3 shows our numerical potentials for  $|a| = \infty$  (solid lines) and finite  $a$  (dashed lines) as well. For  $a > 0$  in Fig 3(a), the effective potentials correspond to the weakly bound channel, converging to the energy of the weakly bound dimer state [Eq. (10)] given approximately by  $-1/ma^2$ . This fact manifests itself at large  $R$  in Fig. 3 by the  $-R^2$  divergence of the curves. As the scattering length grows in magnitude, the effective potential should converge to the Efimov potential (indicated by the horizontal dashed line) in the range  $r_0 \ll R \ll |a|$ .

Similarly, Fig. 3(b) shows the  $a < 0$  effective potentials corresponding to the lowest continuum channel and converging to the Efimov potential when  $|a| \rightarrow \infty$  (horizontal dashed line). For finite  $a$ , this curve must asymptotically approach the lowest kinetic energy eigenvalue (dotted line)  $-\lambda(\lambda+4)+4$  with  $\lambda = 0$ . The lowest effective potential converges to the deeply bound dimer state and is omitted. Efimov states in this case are thus resonances rather than bound states, since they can decay to the lower-energy dimer channels [8].

The vertical lines in Fig. 3 correspond to  $R = r_0$  and  $R = |a|$ , with  $|a| = 500, 10000, 100000$  and  $200000$  a.u.. Within this region — actually  $r_0 \ll R \ll |a|$  — the associated potential is expected to be universal, i.e., behave like the Efimov potential. Clearly, the potentials do not satisfy this expectation over the whole range of  $r_0 \leq R \leq |a|$  as is often assumed. Instead, the condition specifies  $R$  “much” greater than  $r_0$  and “much” less than  $|a|$ .

If we arbitrarily establish a limiting relative error of 10% in the comparison between the finite scattering length potential, as plotted in Fig. 3, and the Efimov potential, then we see that for positive scattering lengths in the range  $20r_0 \lesssim R \lesssim |a|/13$  the effective potentials can be considered an Efimov potential. For  $a \leq 30000$  a.u., however, the effective potential does not come within 10% of the Efimov potential in the range  $r_0 \leq R \leq a$ . For negative scattering lengths, the effective potentials can be considered (with an error of 10%) to be an Efimov potential in the range  $33r_0 \lesssim R \lesssim |a|/13$ . Thus, both

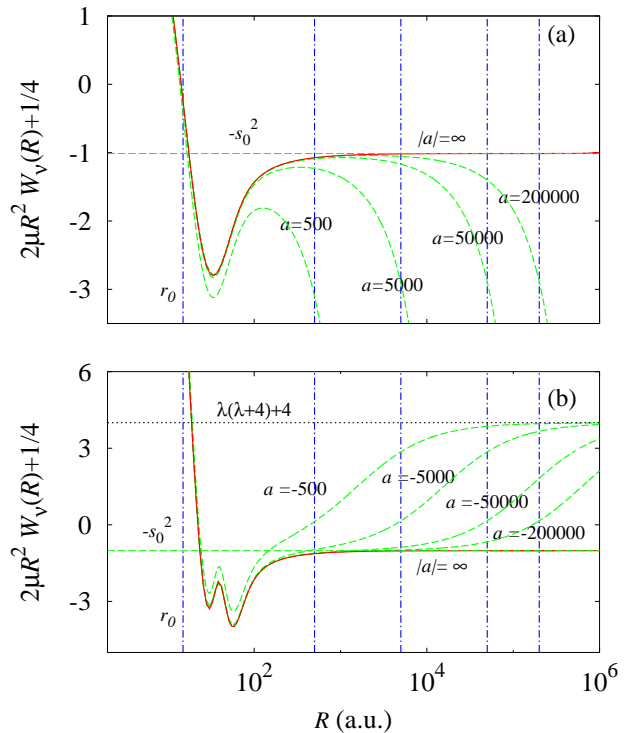


FIG. 3: Three-body effective potentials for (a)  $a > 0$  and (b)  $a < 0$ , with  $|a| = 500, 10000, 100000$ , and  $200000$  a.u. (dashed lines). Also shown is the numerical result for  $|a| = \infty$  (solid line). The horizontal dashed line at  $-s_0^2$  is the Efimov potential, Eq. (12), and the vertical lines correspond to  $R = r_0$  and  $R = |a|$ .

positive and negative  $a$  results are reasonably consistent with the assumption that the Efimov result holds for  $r_0 \ll R \ll |a|$ , but are not consistent with  $r_0 \lesssim R \lesssim |a|$ . Since the standard estimate for the number of Efimov states, Eq. (14), assumes that the Efimov potential holds in the full range of  $R$  from  $r_0$  to  $|a|$ , these more restrictive ranges reduce the estimated number of Efimov states by about 2.

For the  ${}^4\text{He}$  three-body problem, for instance, where  $a \simeq 170$  a.u., the effective potential does not approach within 10% of the Efimov potential in the range  $r_0 \leq R \leq a$ . The above-mentioned restrictions lead to the conclusion that no Efimov state should occur in this case. Nevertheless, accurate numerical calculations predict a single Efimov state [20], which agrees with the result obtained using Eq. (14) where no such restrictions were imposed. Therefore, despite the more restrictive assumptions discussed here, Efimov physics can still be observed — even when the effective potential does not approach the Efimov potential. The potentials are still modified in the range  $r_0 \lesssim R \lesssim |a|$ , just not as dramatically. This modification can be seen in Fig. 3 for  $a = 500$ , where the curve shows a pronounced maximum near  $R = 100$  a.u. before assuming its asymptotic behavior. This sort of deviation seems to indicate the influence of Efimov physics — the

smaller this feature, the weaker the influence.

In Fig. 4 we show the effective potential for the Efimov channel with  $|a| = \infty$  for systems with different numbers of  $s$ -wave bound states. The labels  $D_I$ ,  $D_{II}$ ,  $D_{III}$  and  $D_{IV}$  denote the two-body potential strengths that produce  $|a| = \infty$  with no  $s$ -wave bound states, and with one, two and three  $s$ -wave bound states, respectively (see Fig. 1). For systems with multiple  $s$ -wave bound states there are also rotationally excited two-body bound states that are included in the numerical calculations. The inset in Fig. 4 shows that the lower limit on the range of validity of the Efimov potential (12) changes with the number of two-body bound states. Therefore, the restriction on the lower limit grows even stronger when the number of bound states increases. For instance, with two  $s$ -wave bound states ( $D_{III}$  in Fig. 4), the lower limit must be set at  $48r_0$  to meet our 10% relative error criterion. Figure 4 also appear to converge to a limiting curve as the number of two-body bound states increases.

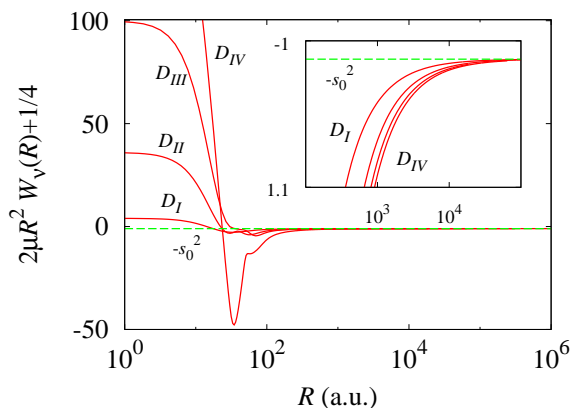


FIG. 4: The attractive dipole effective potential for different number of two-body bound states.  $D_I$ ,  $D_{II}$ ,  $D_{III}$  (as given in Fig. 1) and  $D_{IV}$  (not shown in Fig. 1) indicates the effective potentials with no  $s$ -wave bound states, and with one, two and three  $s$ -wave bound states, respectively.

It is interesting to notice that for  $|a| \rightarrow \infty$  the continuum channels also reflect Efimov physics. While they still represent three free particles, they also include some sort of correlation in addition to the kinetic energy. Figure 5 shows the effective potentials for the continuum channels with  $|a| = \infty$  (solid lines) and  $a = 8000$  a.u. (dashed lines). As  $R \rightarrow \infty$ , the curves for finite  $a$  approach the eigenvalues of the kinetic energy  $\lambda(\lambda + 4) + 4$  (the dotted lines in Fig. 5). The effective potentials for  $|a| = \infty$ , however, converge to a different limit when  $R \rightarrow \infty$ , and can be determined analytically [1]. From Fig. 5, we can see that some of the curves for  $|a| = \infty$  still converge to the kinetic energy eigenvalues. Generally, these curves are degenerate in  $\lambda$  with  $l_0 \neq 0$  — only states that have primarily  $s$ -wave two-body character are impacted by Efimov physics. As was the case for the attractive dipole potential, the effective potentials for the continuum channels with finite  $a$  behave like the Efimov

potentials [Eq. (13)] in the range  $r_0 \ll R \ll |a|$ . In fact, these modifications to the effective potentials have been seen for other three-body systems (also for higher partial waves) and have been shown to play a fundamental role in the scattering length scaling laws of ultracold three-body collisions [13].

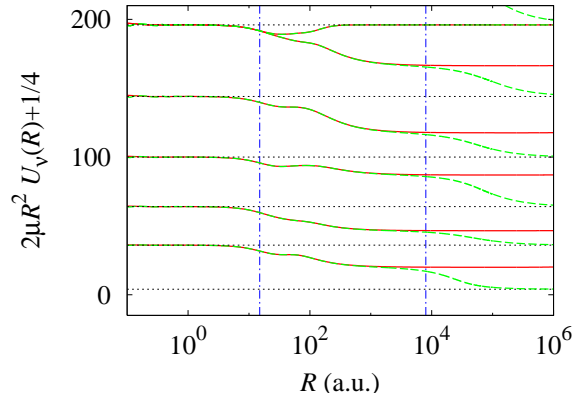


FIG. 5: Three-body effective potentials associated with the continuum channels for  $|a| = \infty$  (solid lines) and for  $a = 8000$  a.u. (dashed lines). The dotted lines correspond to the eigenvalues of the kinetic energy; and the vertical dot-dashed lines to the boundaries  $r_0$  and  $a$ .

## B. Channel Functions

In Fig. 6 we show the channel functions for the three classes of states: bound (BC), continuum (CC), and Efimov (EC). For the  $J^\pi = 0^+$  symmetry, the channel functions do not depend on the Euler angles; they can thus be visualized for fixed values of  $R$  as a function of the hyper-angles  $\varphi$  and  $\theta$  only. We show only one third of the range of  $\varphi$  in Fig. 6 since the rest of the wave function can be obtained by symmetry:  $\Phi(\varphi + 4\pi/3) = \Phi(\varphi + 2\pi/3) = \Phi(\varphi)$ . Further, we show the region that includes  $r_{13} = 0$  — this point lies at  $\varphi = \pi/3$  and  $\theta = \pi/2$ . The hyperangular distribution tells us about the geometry of the system. At  $\theta = 0$ , for instance, the atoms form an equilateral triangle and at  $\theta = \pi/2$  they lie along a line.

As  $R$  increases, a bound channel function collapses like  $R^{-1}$  to the region around  $r_{ij} = 0$ , as shown in the first row of Fig. 6 for  $a = 500$  a.u.. The channel function occupies a smaller and smaller region of the  $(\varphi, \theta)$  plane as  $R$  increases, so must grow in amplitude to preserve normalization. The second row of Fig. 6 represents the lowest continuum channel function for  $a = 500$  a.u., which is the second channel for the system. Therefore, the channel function must approach the  $\lambda = 0$  hyperspherical harmonic (a constant function of the hyperangles) as  $R \rightarrow \infty$ , and it must have one node (careful inspection of the figure near  $\theta = 0$  shows that  $\Phi < 0$ ). In Fig. 6 the harmonic character is easily seen since the channel function is spread nearly uniformly over the entire

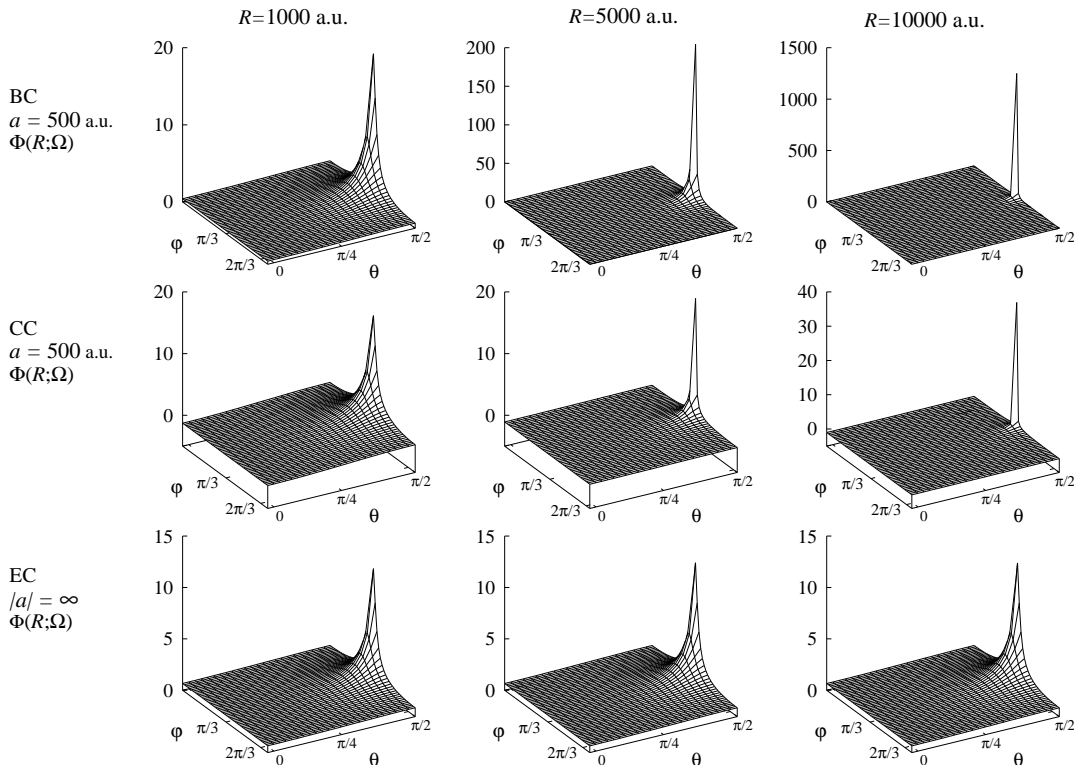


FIG. 6:  $J^\pi = 0^+$  channel functions  $\Phi(R; \Omega)$  for fixed values of the hyperradius  $R$ . The first and second lines show the bound channel (BC) and the lowest continuum channel (CC) for  $a = 500$  a.u.. The third line shows the Efimov channel (EC), demonstrating that it is insensitive to changes in  $R$ .

hyperangular plane. It is also apparent that there is a substantial amplitude at the two-body coalescence point and that this amplitude shrinks with growing hyperradius just as for the bound channel.

The last row of Fig. 6 shows the channel function for  $|a| = \infty$ . These channel functions share characteristics of both the bound and continuum channels. That is, they have large amplitude at the two-body coalescence points, but they are also spread over the entire plane. These channel functions, however, have one important characteristic that the others do not have: they are nearly scale invariant. That is, they look essentially the same at every value of  $R$ . This scale invariance is, in fact, one of the defining properties of the Efimov effect. These channel functions also show why the Efimov effect is so tenuous — the three bodies must maintain a delicate balance between the two-body and three-body parts of configuration space over ever-growing volumes of space. If there are two-body bound states present, this Efimov channel function will acquire nodes closely resembling those of the continuum channel.

In Fig. 7 we compare the channel functions for the weakly bound channel for  $a = 500$  a.u.,  $a = 1000$  a.u., and  $|a| = \infty$  at  $R = 10000$  a.u.. This figure shows

the channel function on a logarithmic scale (in the  $z$ -direction) to emphasize the delocalization in the Efimov case ( $|a| = \infty$ ). At this value of  $R$ , the delocalization grows with  $a$ , while all cases have large amplitude at the two-body coalescence points.

### C. Nonadiabatic couplings

The asymptotic behavior of the nonadiabatic coupling for finite  $a$  has been deduced analytically for all combinations of bound and continuum channels [19]. The coupling to the Efimov channel, however, was only briefly discussed [21], and that was only for the diagonal coupling element  $Q_{\nu\nu}$ . We have found that the nonadiabatic coupling is also modified due to Efimov physics in the range  $r_0 \ll R \ll |a|$ . In Table I we show the leading term in the asymptotic expansions of  $P_{\nu\nu'}$  and  $Q_{\nu\nu'}$  couplings deduced in Ref. [19] which are expected to be valid for  $R \gg |a|$ . Here, we will restrict our analysis to couplings between  $s$ -wave channels and the Efimov channel. The numerically calculated couplings were obtained for values of the interaction strength near  $D = D_{II}$  (Fig. 1), where the system has one bound state for  $a < 0$  and

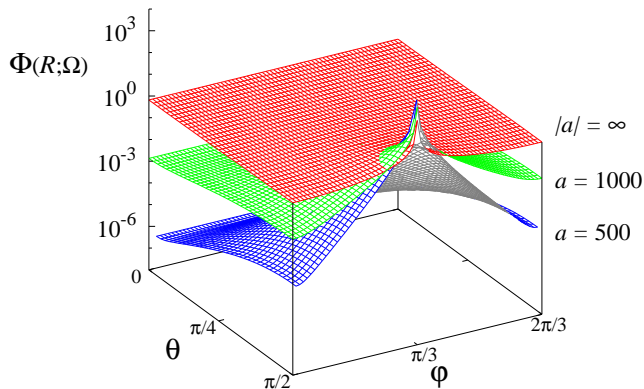


FIG. 7: Channel function for the weakly bound channel at  $R = 10000$  a.u. for  $a = 500$  a.u. and  $a = 1000$  a.u.. The  $|a| = \infty$  channel function is also shown for comparison. Note that the vertical scale is logarithmic.

two bound states for  $a > 0$ . In this case, therefore, we investigate the behavior of the nonadiabatic coupling in a situation similar to crossing an  $s$ -wave Feshbach resonance [2, 3, 4, 5, 6], which involves the formation of a weakly bound molecule for  $a > 0$ .

$\nu - \nu'$	$P_{\nu\nu'}(R)$	$Q_{\nu\nu'}(R)$
BC( $l = 0$ )–BC( $l = 0$ )	$R^{-1}$	$R^{-2}$
BC( $l = 0$ )–CC( $l_0 = 0$ )	$R^{-5/2}$	$R^{-7/2}$
CC( $l_0 = 0$ )–CC( $l_0 = 0$ )	$R^{-2}$	$R^{-4}$

TABLE I: The leading term for the asymptotic expansion of the nonadiabatic coupling involving bound channels (BC) and continuum channels (CC). The diagonal coupling  $Q_{\nu\nu}$  for BC is proportional to  $R^{-2}$ , while for CC it is proportional to  $R^{-4}$  (see Ref. [19]).

We plot in Figs. 8, 9, and 10 the numerically calculated nonadiabatic couplings on a log-log scale in order to highlight the expected power law behavior. Figure 8 shows the couplings between an  $s$ -wave bound channel and the Efimov channel for finite  $a$  (dashed lines) and  $|a| = \infty$  (solid line). For  $a > 0$ , and  $R \gg a$ , the couplings behave as couplings between bound channels, given in Table I. For  $a < 0$ , they behave as couplings between bound and continuum channels. As  $|a| \rightarrow \infty$ , the couplings in both Figs. 8(a) and (b) approach a limiting value given by the  $|a| = \infty$  result. In the range  $r_0 \ll R \ll |a|$ , indicated in Fig. 8 by the vertical dot-dashed lines, the couplings are modified due to Efimov physics. The  $|a| = \infty$  coupling at the other poles of Fig. 1 will have the same behavior for  $R \gg r_0$ , but the short-range behavior will differ.

Figure 9 shows the coupling between the Efimov channel and the lowest continuum channel for  $a > 0$  and the next continuum channel for  $a < 0$ . The  $a > 0$  curves

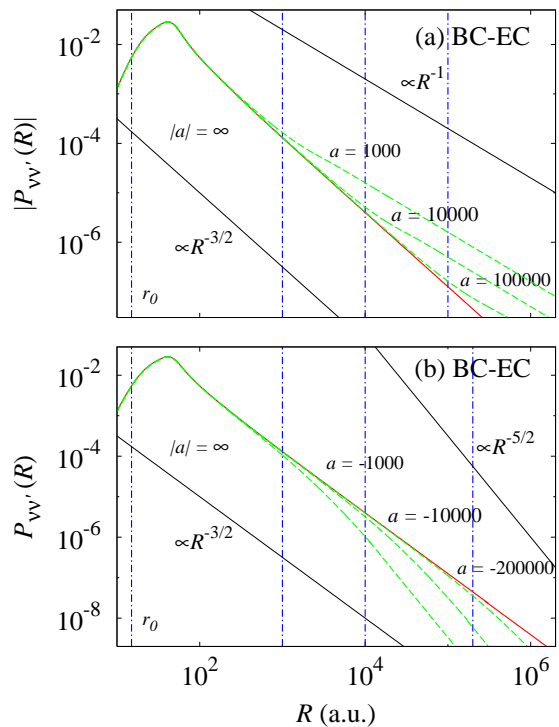


FIG. 8: The nonadiabatic couplings between a bound channel and the Efimov channel for finite (dashed lines) and infinite (solid line) scattering lengths. For  $a > 0$  (a) the Efimov channel is associated with the weakly bound channel; and for  $a < 0$  (b) with the lowest continuum channel.

in Fig. 9(a) show the characteristic peak around  $R \simeq 3a$  predicted in [11] responsible for three-body recombination at ultracold temperatures. For  $a < 0$ , there is one node at the dip in Fig. 9(b) (since the absolute value was taken for this plot). As  $|a|$  increases, the node moves to infinity, and the coupling for the Efimov case emerges.

The asymptotic behavior of the diagonal correction in Fig. 10 also confirms the results in Ref. [19] for finite  $a$ . In Fig. 10 the diagonal coupling for  $|a| = \infty$  is proportional to  $R^{-3}$ , which lies between the  $R^{-2}$  expected for  $a > 0$  and  $R^{-4}$  expected for  $a < 0$  (see Table I).

Our calculations confirm all of the finite  $|a|$  asymptotic analysis of Ref. [19]. Table II summarizes the cases for coupling with the Efimov channel when  $|a| = \infty$ . It shows the leading term in the expansion of the nonadiabatic couplings for three identical bosons and are expected to be valid in the range  $r_0 \ll R \ll |a|$ , as with the other results related to Efimov physics. Since the continuum channels are also modified due to the Efimov physics (see Fig. 5), the couplings between bound channels and the continuum channels are expected to change. In fact, only the coupling between  $s$ -wave bound channels and continuum channels with  $l_0 = 0$  are different from the finite  $a$  case. We have included this coupling in the last line of Table II for completeness.

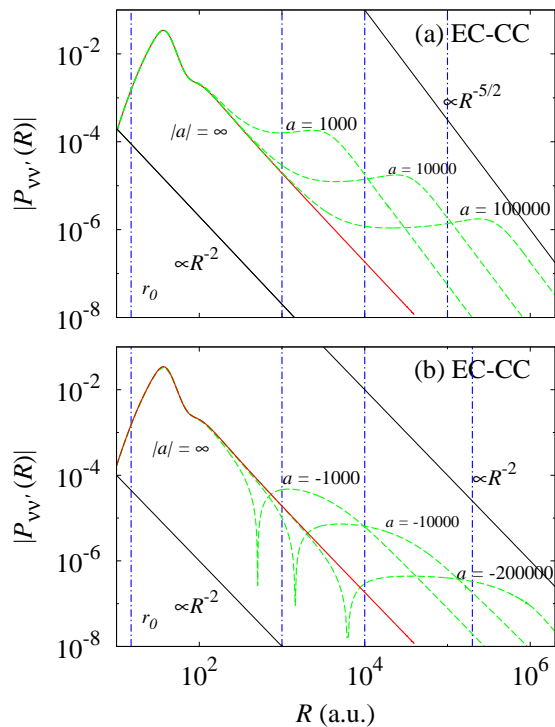


FIG. 9: The nonadiabatic couplings between the Efimov channel and a continuum channel for finite (dashed lines) and infinite (solid line) scattering lengths. For  $a > 0$  (a) the Efimov channel is associated with the weakly bound channel; and for  $a < 0$  (b) with the lowest continuum channel.

$\nu - \nu'$	$P_{\nu\nu'}(R)$	$Q_{\nu\nu'}(R)$
EC-BC( $l = 0$ )	$R^{-3/2}$	$R^{-5/2}$
EC-CC( $l_0 = 0$ )	$R^{-2}$	$R^{-3}$
BC( $l = 0$ )-CC( $l_0 = 0$ )	$R^{-3/2}$	$R^{-5/2}$

TABLE II: The leading term for the asymptotic expansion of the nonadiabatic couplings for  $|a| = \infty$ . The diagonal coupling  $Q_{\nu\nu}$  for the Efimov channel is proportional to  $R^{-3}$ .

Comparing Tables I and II, we see that the Efimov channel shares characteristics of bound and continuum channels. The coupling between the Efimov channel and bound channels ( $R^{-3/2}$ ) falls faster than the coupling between bound channels ( $R^{-1}$ ), but slower than the coupling between bound and continuum channels ( $R^{-5/2}$ ). The coupling between the Efimov channel and continuum channels ( $R^{-2}$ ) falls faster than the coupling between bound and continuum channels ( $R^{-5/2}$ ), but, is the same as the coupling between continuum channels ( $R^{-2}$ ).

From Figs. 8, 9 and 10 it is clear that the couplings for finite  $a$  also exhibits universal aspects. This universal behavior would better seen by plotting  $|a|P_{\nu\nu'}(R/|a|)$  and  $|a|^2Q_{\nu\nu'}(R/|a|)$ . In such a plot the couplings for different values of  $a$  look all the same for  $R/|a| \gg 1$ .

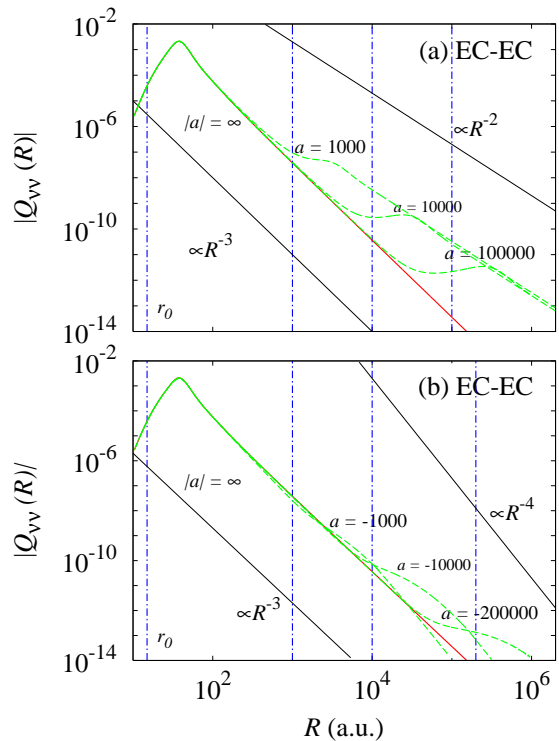


FIG. 10: The diagonal nonadiabatic coupling for the Efimov channel for finite (dashed lines) and infinite (solid line) scattering lengths. For  $a > 0$  (a) the Efimov channel is associated with the weakly bound channel; and for  $a < 0$  (b) with the lowest continuum channel.

#### IV. SUMMARY

We have investigated several fundamental aspects of Efimov physics in the hyperspherical adiabatic representation of systems of three identical bosons. We have calculated effective hyperspherical potentials for very large to infinite values of the two-body  $s$ -wave scattering length. These calculations were obtained in a regime not accessible in previous calculations, allowing us to test assumptions related to the Efimov effect, namely, the emergence of the long-range three-body effective interactions in the range where  $r_0 \ll R \ll |a|$ . Our results show that despite the more restrictive limits discussed here for the effective potentials, the assumption that the long-range attractive potential holds in the range  $r_0 \lesssim R \lesssim |a|$  gives a good qualitative description of the Efimov physics. In fact, for  $a \gtrsim r_0$ , the unrestricted result for the number of Efimov states seems to give a better description, even though the effective potential does not resemble the Efimov potential. Additionally, we have shown that as we increase the number of two-body bound states the effective potential seems to converge to a limiting curve.

We have also obtained the behavior of many other quantities affected by Efimov physics: the continuum effective potentials, all of the nonadiabatic couplings with

the Efimov channel, and the channel functions themselves. As expected, the channel functions are essentially unchanged with  $R$ . Moreover, the nonadiabatic couplings reveal that the Efimov channel behaves in some ways like a bound state and in others like a continuum state. We have quantified these different regimes and verified that the effects are limited to  $r_0 \ll R \ll |a|$  for all quantities.

## Acknowledgments

This work was supported by the National Science Foundation and by the Research Corporation.

- 
- [1] V. Efimov, *Sov. J. Nucl. Phys.* **12**, 589 (1971); **29**, 546 (1979); *Nucl. Phys. A* **210**, 157 (1973).
  - [2] S. Inouye *et al.*, *Nature (London)* **392**, 151 (1998).
  - [3] Ph. Courteille *et al.*, *Phys. Rev. Lett.* **81**, 69 (1998).
  - [4] J. L. Roberts *et al.*, *Phys. Rev. Lett.* **81**, 5109 (1998).
  - [5] P. G. Kevrekidis, G. Theocharis, D. J. Frantzeskakis, and B. A. Malomed, *Phys. Rev. Lett.* **90**, 230401 (2003).
  - [6] T. Weber *et al.*, *Phys. Rev. Lett.* **91**, 123201 (2003).
  - [7] B. D. Esry, C. H. Greene and J. P. Burke, *Phys. Rev. Lett.* **83**, 1751 (1999).
  - [8] E. Nielsen, H. Suno, and B. D. Esry, *Phys. Rev. A* **66**, 012705 (2002).
  - [9] E. Braaten, H. -W. Hammer, and M. Kusunoki, *Phys. Rev. Lett.* **90**, 170402 (2003); *Phys. Rev. A* **67**, 022505 (2003); E. Braaten and H.-W. Hammer, *Phys. Rev. A* **70**, 042706 (2004); E. Braaten, H.-W. Hammer, and T. Mehen, *Phys. Rev. Lett.* **88**, 040401 (2002).
  - [10] E. Braaten and H. -W. Hammer, *cond-mat/041017*.
  - [11] E. Nielsen and J. H. Macek, *Phys. Rev. Lett.* **83**, 1566 (1999).
  - [12] J. P. D’Incao, H. Suno, and B. D. Esry, *Phys. Rev. Lett.* **93**, 123201 (2004).
  - [13] J. P. D’Incao and B. D. Esry, *cond-mat/0411565*.
  - [14] A. Bulgac, *Phys. Rev. Lett.* **89**, 050402 (2002).
  - [15] H. Suno, B. D. Esry, C. H. Greene and J. P. Burke, Jr., *Phys. Rev. A* **65**, 042725 (2002).
  - [16] H. Suno, B. D. Esry, and C. H. Greene, *New J. Phys.* **5**, 53 (2003).
  - [17] B. R. Johnson, *J. Chem. Phys.* **73**, 5051 (1980); R. C. Whitten and F. T. Smith, *J. Math. Phys.* **9**, 1103 (1968);
  - [18] Z. Zhen and J. Macek, *Phys. Rev. A* **38**, 1193 (1988).
  - [19] E. Nielsen, D. V. Fedorov, A. S. Jensen, and E. Garrido, *Phys. Rep.* **347**, 373 (2001).
  - [20] B. D. Esry, C. D. Lin, and C. H. Greene, *Phys. Rev. A* **54**, 394 (1996); E. Nielsen, D. V. Fedorov, and A. S. Jensen, *J. Phys. B.* **31**, 4085 (1998); E. Braaten and H.-W. Hammer, *Phys. Rev. A* **67**, 042706 (2003).
  - [21] D. V. Fedorov and A. S. Jensen, *Phys. Rev. Lett.* **71**, 4103 (1993).